Force Titration of Langmuir−Blodgett Bilayers of Glycine Amphiphiles: JKR-Type Measurements Using the Surface-Force Apparatus

James Schneider,*,† Yoav Dori, Kraig Haverstick, and Matthew Tirrell*,‡

Department of Chemical Engineering and Materials Science, University of Minnesota, Minneapolis, Minnesota 55455

Ravi Sharma

Materials Science and Engineering Division, Eastman Kodak Company, Rochester, New York 14650-2158

Received September 28, 2001. In Final Form: January 10, 2002

Using the surface-force apparatus, we have made Johnson−Kendall−Roberts (JKR)-type adhesion measurements between Langmuir−Blodgett (LB) bilayers of a novel glycine amphiphile. The bilayers show a pronounced adhesion hysteresis at low pH that is completely removed at high pH. The adhesion hysteresis is marked by a spatially varying adhesion gradient on unloading that can be explained in terms of pH-dependent jump-to-contact forces. In addition to providing some insight into the mechanisms of interfacial bonding in biological systems, the JKR technique applied to LB bilayers of peptide amphiphiles emerges as a novel, quantitative method for fundamental bioadhesion measurements.

Introduction

The understanding of adsorption and adhesion in biological processes such as cell adhesion[1,2] and protein adsorption[3] has been limited by a lack of quantitative knowledge concerning the molecular-level van der Waals, electrostatic, and hydrogen-bonding interactions occurring at these interfaces.[4] Acid−base interactions,[5] which involve associations between ionizable surface-bound groups in electrolyte solutions, are particularly pertinent to biological systems owing to the abundance of carboxyl and amine groups in proteins.[6] One approach toward the greater quantification and understanding of these interfacial processes has been to characterize model functionalized surfaces constructed by self-assembly or Langmuir−Blodgett deposition.[7] Techniques such as surface-enhanced Raman spectroscopy[8] and contact-angle titration[9,10] have been used to measure the extent of surface charging in these model systems. Direct force measurement techniques, such as atomic force microscopy (AFM)[11] and surface-force apparatus (SFA)[12] measurements, can potentially provide more information by assessing out-of-contact electrostatic interactions as well as in-contact adhesion, to which hydrogen bonding may be a sizable contributor.

The term "force titration" has been used to describe AFM-derived adhesion measurements between self-assembled monolayers (SAMs) as a function of pH.[13] Force titration measurements on carboxylic acid (−COOH) and amine-terminated ($-NH_3$) SAMs have shown some interesting behavior.[13−19] Generally speaking, at moderate to high ionic strength the adhesion between −COOH SAMs decreases sigmoidally to zero as pH is increased, while $-NH_3$ SAMs have a sigmoidally increasing adhesion with pH. The pH midpoint of these titrations varied substantially from one study to another, but typically the values for the −COOH systems were about 1−2 pH units higher than the free solution value of 4.75 for fatty acids.[20] The difference can be attributed to several mechanisms, including the lowering of the surface pH relative to the bulk by surface charging. This has the effect of broadening the titration curve and shifting midpoint pH to higher

* Corresponding authors.
† Current address: Department of Chemical Engineering, Carnegie Mellon University, Pittsburgh PA 15213-3890.
‡ Current address: Departments of Chemical Engineering and of Materials, University of California, Santa Barbara CA 93106.

(1) Hammer, D. A.; Tirrell, M. *Annu. Rev. Mater. Sci.* **1996**, *26*, 651−691.
(2) Fletcher, M. Bacterial Attachment in Aquatic Environments: A Diversity of Surfaces and Adhesion Strategies. In *Bacterial Adhesion*: *Molecular and Ecological Diversity*; Fletcher, M., Ed.; John Wiley and Sons: New York, 1996.
(3) Prime, K. L.; Whitesides, G. M. *J. Am. Chem. Soc.* **1993**, *115*, 10714−10721.
(4) Israelachvili, J. N. *Intermolecular and Surface Forces*; Academic Press: New York, 1992.
(5) Whitesides, G. M.; Biebuyck, H. A.; Folkers, J. P.; Prime, K. L. Acid−Base Interactions in Wetting. In *Acid−Base Interactions*; Mittal, K. L., Anderson, H. R., Eds.; VSP: New York, 1991.
(6) Creighton, T. E. *Proteins*: *Structures and Molecular Properties*; W. H. Freeman: New York, 1993.
(7) Ulman, A. *An Introduction to Ultrathin Organic Films*; Academic Press: New York, 1991.
(8) Mullen, K. I.; Wang, D. X.; Crane, L. G.; Carron, K. T. *Anal. Chem.* **1992**, *64*, 930−936.
(9) Holmes-Farley, S. R.; Reamey, R. H.; McCarthy, T. J.; Deutch, J.; Whitesides, G. M. *Langmuir* **1985**, *1*, 725−740.
(10) Wasserman, S. R.; Tao, Y.-T.; Whitesides, G. M. *Langmuir* **1989**, *5*, 1074−1087.
(11) Frisbie, C. D.; Rozsnyai, L. F.; Noy, A.; Wrighton, M. S.; Lieber, C. M. *Science* **1994**, *265*, 2071−2074.
(12) Leckband, D. *Nature* **1995**, *376*, 617−618.
(13) Vezenov, D. V.; Noy, A.; Rozsnyai, L. F.; Lieber, C. M. *J. Am. Chem. Soc.* **1997**, *119*, 2006−2015.
(14) Vegte, E. W.v.d.; Hadziioannou, G. *J. Phys. Chem. B* **1997**, *101*, 9563−9569.
(15) Kane, V.; Mulvaney, P. *Langmuir* **1998**, *14*, 3303−3311.
(16) He, H.-X.; Huang, W.; Zhang, H.; Li, Q. G.; Li, S. F. Y.; Liu, Z. F. *Langmuir* **2000**, *16*, 517−521.
(17) Kokkoli, E.; Zukoski, C. F. *Langmuir* **2000**, *16*, 6029−6036.
(18) Smith, D. A.; Wallwork, M. L.; Zhang, J.; Kirkham, J.; Robinson, C.; Marsh, A.; Wong, M. *J. Phys. Chem. B* **2000**, *104*, 8862−8870.
(19) Wei, Z. Q.; Wang, C.; Zhu, C. F.; Zhou, C. Q.; Xu, B.; Bai, C. L. *Surf. Sci.* **2000**, *459*, 401−412.
(20) Lide, D. R. *CRC Handbook of Chemistry and Physics*; CRC Press: Boca Raton, FL, 1991.

10.1021/la011496g CCC: $22.00
Published on Web 02/08/2002

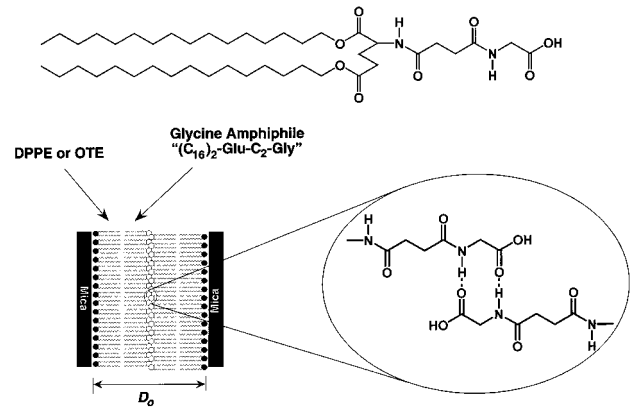

Figure 1. Structure of the $(C_{16})_2$-Glu-C_2-Gly molecule ("glycine amphiphile") and its position in the composite bilayer. The monolayer nearest the mica surface is either DPPE or OTE (see text). All amphiphiles are deposited in the liquid-condensed region, below their melting transition temperature.

values.[14,15] Kane and Mulvaney[15] uncovered an inconsistency between surface potential data calculated from out-of-contact force data and those from adhesion data within a surface dissociation model. The discrepancy was ascribed to either the existence of an ion-impermeable Stern layer or the adsorption of sodium ions to the surface, lowering the surface potential. Further complicating these studies, Smith et al.[18] observed maxima in −COOH force titrations performed at low ionic strength, which were explained by the existence of stronger COO−/COOH hydrogen bonds that are screened by dense, high-salt double layers. A competition between in-plane and out-of-plane hydrogen bonds acting to impede deprotonation has also been discussed.[14]

Despite the considerable insight these studies have provided, the carboxylic acid SAM results are difficult to interpret, in part because the ionizable group is the same as the hydrogen-bonding group. We have been investigating a system that can be considered more biologically relevant and, additionally, has distinct ionizable groups and hydrogen-bonding groups.[21−23] In a previous work,[23] we performed force titration experiments using the SFA on Langmuir−Blodgett (LB) layers[7] of a novel synthetic glycine amphiphile (Figure 1). Like the alkanethiol SAMs discussed above, these LB layers are highly ordered and their molecular functionality can be tailored by depositing functional variants onto surfaces prior to analysis.

Our previous work[21−23] has shown that LB layers of glycine amphiphiles adhere to each other strongly at pH 5.6 ($-(F/R)_0 = 80 \pm 5$ mN/m) but do not adhere at a pH greater than 8.0. SFA force profiles measured between the glycine bilayers over this pH range (Figure 2) show exponentially increasing double-layer repulsion whose magnitude increases with pH as the terminal carboxylic acids deprotonate. At moderate pH, the bilayers are torn apart on separation to maintain headgroup/headgroup contact, roughening the surfaces and giving rise to additional steric repulsive forces on second approach. At high pH (8.0 and above), the adhesion is extinguished.

Close inspection of the pH dependence of the adhesion (Figure 3) revealed that the increased electrostatic repulsion at higher pH does not fully account for the decrease

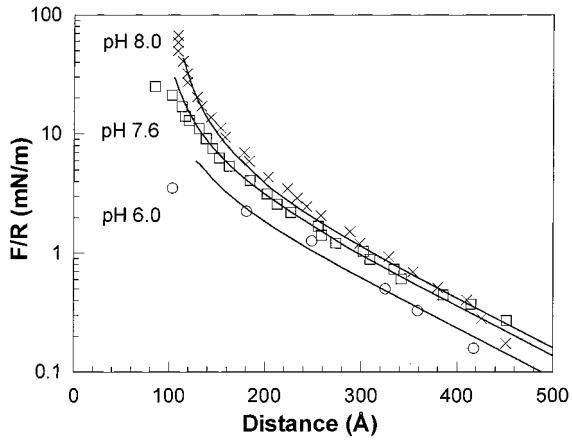

Figure 2. SFA force profiles for glycine bilayers in 1 mM KBr at pH 6.0, 7.6, and 8.0, demonstrating a steadily increasing electrostatic repulsion with increasing pH. The lines are constant-charge solutions of the Poisson−Boltzmann equation using the algorithm of Chan et al. (ref 49), with the origin of charge set at 15 Å beyond the contact separation distance to account for in-contact headgroup interpenetration at pH 6.0 and pH 7.6.

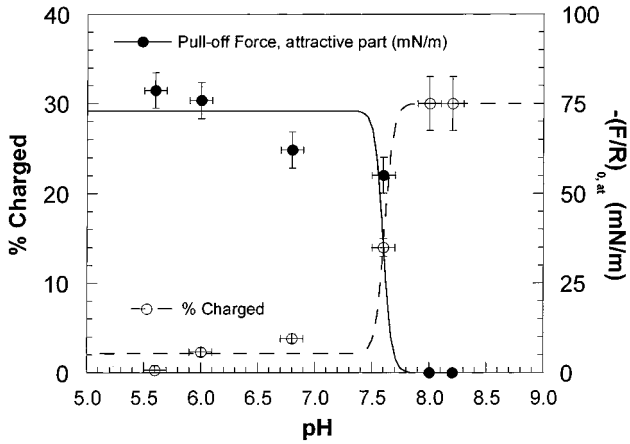

Figure 3. Summary of SFA data collected on the glycine bilayers from a previous work (ref 23). The "%Charged" data were obtained from fitting out-of-contact SFA force profiles to a solution to the Poisson−Boltzmann expression. The attractive part of the pull-off force ($-(F/R)_{0,at}$) was calculated by adding the electrostatic double-layer repulsion to the measured pull-off force. The coincidence of the two curves indicates that charge-induced blocking of short-range attractive forces also acts to attenuate adhesion. Lines are to guide the eye.

in adhesion, so that charging must also act to block the formation of interlayer hydrogen bonds. Furthermore, the low-pH adhesion was accompanied by a 15 Å decrease in the in-contact bilayer thickness (D_0, Figure 1). This decrease was ascribed to headgroup interpenetration, exposing amine groups to the interface for interlayer hydrogen bonding. We concluded that the effect of added surface charge was to block the interpenetration required for strong adhesion. This model was supported by measurements made on functional variants of the glycine amphiphile.

Here, we explore the formation and breakage of the adhesive contact as a function of pH by a Johnson−Kendall−Roberts (JKR)-type analysis[24] using the SFA. The SFA optical techniques yield absolute measurements of intersurface separation distance and contact area, which can be interpreted within JKR theory. Ångstrom-level

(21) Schneider, J.; Dori, Y.; Tirrell, M.; Sharma, R. *Thin Solid Films* **1998**, *329*, 772−777.
(22) Schneider, J.; Berndt, P.; Haverstick, K.; Kumar, S.; Chiruvolu, S.; Tirrell, M. *J. Am. Chem. Soc.* **1998**, *120*, 3508−3509.
(23) Schneider, J.; Berndt, P.; Haverstick, K.; Kumar, S.; Chiruvolu, S.; Tirrell, M. *Langmuir*, submitted.
(24) Johnson, K. L.; Kendall, K.; Roberts, A. D. *Proc. R. Soc. London, Ser. A* **1971**, *324*, 301−313.

measurements of separation distance are achieved by tracking the wavelength position of a multiple-beam interference pattern known as "fringes of equal chromatic order" (FECO).[25] The FECO fringes have a characteristic "C" shape reflecting the curvature of the mica substrates. The FECO flatten when the substrates are in contact, and the size of the flattened region is equal to the contact diameter within an optical calibration constant. The contact area can be monitored while contacted surfaces are further loaded or unloaded, in this case with micron-scale resolution.

Johnson et al.[24] developed a relationship between the contact area and the applied load for elastic bodies in adhesive contact. Their "JKR theory" balanced mechanical and potential energy with the adhesion energy (W) required to create additional interface. The application of this theory made possible the interpretation of sensitive adhesion measurements on curved samples. For the crossed-cylinders geometry of the SFA, the JKR working equation is

$$a^3 = \frac{R}{K}(P + 3\pi WR + \sqrt{6\pi WRP + (3\pi WR)^2}) \quad (1)$$

where a is the radius of the circular contact, R is the mean radius of curvature, and K is an elasticity constant related to the deformation moduli of the substrates. Using the values for R and a obtained by analysis of the FECO, a two-parameter fit of eq 1 can be made on loading and unloading data to simultaneously specify W and K. JKR theory predicts that complete surface separation, or "pull-off" (subscript 0) will occur under the following conditions:

$$P_0 = -\frac{{a_0}^3 K}{R} = -\frac{3\pi WR}{2} \quad (2)$$

where P_0 and a_0 are the load and contact radius just before pull-off.

By studying the mechanics of the crack fracturing just outside the contact area, Barquins and Maugis[26] showed that the results of JKR theory were more widely applicable to the case of quasi-equilibrium propagation of this crack, substituting for W the strain energy release rate (G), the potential energy that is released from the bulk material as the interfacial crack extends by a unit area. Generally speaking, $G = W$ for loading processes, while G is often much greater than W for unloading processes with strong adhesion. This is due to dissipative effects encountered as strongly bonded material is separated on unloading.

JKR measurements made using functionalized poly(dimethylsiloxane) (PDMS) lenses have been a powerful tool for fundamental adhesion studies,[27−33] but JKR measurements using the SFA give more information, including force−distance profile and the shape of the surfaces in contact. Using the SFA, JKR-type measurements have been made between bare mica samples,[34,35] Langmuir−Blodgett monolayers,[36] thin polymer films,[37] and gold−thiol self-assembled monolayers,[38] yielding values for surface energy that agree well with those obtained from wetting studies in many cases. These results have demonstrated that JKR theory provides a good description of the relationship between surface energy and pull-off force as well as the shape of the deformed surfaces.[39] For these measurements, an effective elastic constant for the multilayer system must be used. Theoretical[40] and experimental[35] work has indicated that the deformation of the glue is not responsible for surface deformation under experimental conditions.

The SFA−JKR approach provides the interfacial energy both as contact is established and as it is broken and also reveals any radial dependence of adhesion in the contact area. This information enables a fuller description of force titration data obtained in this glycine system, whose behavior can be applied broadly to the contributions of hydrogen bonding and electrostatics in biological systems. To our knowledge, these are the first JKR-type measurements made between Langmuir−Blodgett bilayers in aqueous systems, which coupled with the synthetic flexibility of the amino acid amphiphile design, introduce a novel platform for precise, quantitative measurements of molecular-level adhesion in biological systems.

Experimental Methods

In the descriptions that follow, all solvents are HPLC grade, and all reagents are ACS grade. "Water" is deionized water purified in a Milli-Q UV Plus unit (Millipore) to a final resistivity of 18.2 MΩ cm. Glassware was cleaned using a 1:1 chloroform/methanol solution or chromate cleaning solution as necessary.

Synthesis of Glycine Amphiphile. The glycine amphiphile $(C_{16})_2$-Glu-C_2-Gly (Figure 1) was synthesized by a multistep procedure.[41] Amphiphile tail groups were synthesized by a carboxylic acid−alcohol condensation reaction. Glycine was coupled to succinic anhydride to form the headgroup, and the two products linked together using carbodiimide chemistry.

Pressure−Area Isotherms. Pressure−area isotherms and LB depositions were carried out using a computer-controlled, liquid-cooled KSV 5000 Langmuir trough in a dust-free laminar flow hood. Surface pressure measurements were made using a platinum Wilhelmy plate. The movement of the barrier was controlled by a computer algorithm that continually decreased the speed of the barrier movement down to 3 mm/min in response to the increase in surface pressure.

LB Technique. Freshly cleaved mica was used exclusively as a deposition substrate. For AFM studies, thin mica disks (diameter, 2.5 cm^2) were held on edge by clean stainless steel tweezers hung onto the dipper. For SFA studies, mica-covered silica lenses were held from the side by clean stainless steel grippers. For the DPPE/$(C_{16})_2$-Glu-C_2-Gly bilayers, the DPPE monolayer was compressed to a deposition pressure (π_{dep}) of 41 mN/m and this surface pressure was maintained for 5 min to equilibrate the film. The mica was then slowly (1 mm/min) lifted through the film, depositing a monolayer of DPPE. The mica was allowed to dry for 15 min before a monolayer of glycine amphiphile was spread and compressed to $\pi_{dep} = 35$ mN/m. After equilibra-

(25) Israelachvili, J. N. *J. Colloid Interface Sci.* **1972**, *44*, 259−272.
(26) Barquins, M.; Maugis, D. *J. Mec. Theor. Appl.* **1982**, *1*, 337−357.
(27) Chaudhury, M. K.; Whitesides, G. M. *Langmuir* **1991**, *7*, 1013−1025.
(28) Chaudhury, M. K.; Whitesides, G. M. *Science* **1992**, *255*, 1230−1232.
(29) Chaudhury, M. K.; Weaver, T.; Hui, C. Y.; Kramer, E. J. *J. Appl. Phys.* **1996**, *80*, 30−37.
(30) Chaudhury, M. K. *Mater. Sci. Eng. Rep.* **1996**, *19*, 97−159.
(31) Chaudhury, M. K. *Curr. Opin. Colloid Interface Sci.* **1997**, *2*, 65−69.
(32) Dillow, A. K.; Ochsenhirt, S. E.; McCarthy, J. B.; Fields, G. B.; Tirrell, M. *Biomaterials* **2001**, *22*, 1493−1505.
(33) Ulman, A.; Choi, G. Y.; Shnidman, Y.; Zurawsky, W. *Isr. J. Chem.* **2000**, *40*, 107−121.
(34) Horn, R. G.; Israelachvili, J. N.; Pribac, F. *J. Colloid Interface Sci.* **1987**, *115*, 480−492.
(35) Christenson, H. K. *Langmuir* **1996**, *12*, 1404−1405.
(36) Chen, Y. L.; Helm, C. A.; Israelachvili, J. N. *J. Phys. Chem.* **1991**, *95*, 10736−10747.
(37) Mangipudi, V.; Tirrell, M.; Pocius, A. V. *Langmuir* **1995**, *11*, 19−23.
(38) Quon, R. A.; Ulman, A.; Vanderlick, T. K. *Langmuir* **2000**, *16*, 3797−3802.
(39) Maugis, D.; Gauthier-Manuel, B. *J. Adhes. Sci. Technol.* **1994**, *8*, 1311−1322.
(40) Sridhar, I.; Johnson, K. L.; Fleck, N. A. *J. Phys. D.: Appl. Phys.* **1997**, *30*, 1710−1719.
(41) Berndt, P.; Fields, G. B.; Tirrell, M. *J. Am. Chem. Soc.* **1995**, *117*, 9515−9522.

tion, the mica substrates were slowly (1 mm/min) lowered through the film until completely submerged. Transfer ratios (measured on large mica sheets, R_t) were 1.00 ± 0.05 for both deposition processes.

For the octadecyltriethoxysilane (OTE)/$(C_{16})_2$-Glu-C_2-Gly bilayers, mica substrates were activated by plasma treatment prior to LB deposition. Following the protocol of Wood and Sharma,[21,42] mica substrates were exposed to a 30 W, 450 mTorr argon/water vapor plasma in a plasma cleaning unit (Harrick, Inc.) for 2 min to form surface hydroxyl groups. During this process, care was taken to purge the plasma chamber several times with filtered argon to minimize contamination. The mica substrates were then moved to the LB trough for OTE deposition. The trough was filled with water adjusted to pH 2 by nitric acid (Aldrich, high purity). OTE (80 μL, 1 mg/mL) in chloroform was spread on the water surface, yielding an initial surface pressure of about 10 mN/m. The surface pressure decreased gradually as islands of OTE formed on the interface; after 45 min, the surface pressure was nearly zero. At this point, the monolayer of OTE islands was compressed to $\pi_{dep} = 25$ mN/m and transferred on the upstroke at 1 mm/min. The OTE−mica substrates were allowed to dry in the hood and transferred to a clean, empty glass desiccator. The desiccator was sealed and placed in an 80 °C oven for 2 h. After cooling, a monolayer of $(C_{16})_2$-Glu-C_2-Gly was transferred onto the OTE as described above. Transfer ratios (R_t) were 0.95 ± 0.01 for OTE and 0.85 ± 0.05 for $(C_{16})_2$-Glu-C_2-Gly.

Surface-Force Apparatus. SFA measurements were carried out using a stainless steel Mark II SFA built at the University of Minnesota, using a double-cantilever leaf spring of spring constant 3.3×10^5 dyn/cm and cylindrically curved silica lenses (radius of curvature, 2 cm). A differential spring mechanism was used to translate the leaf spring and its lens with nanometer precision. Images of the FECO interference fringes were obtained using a liquid-cooled CCD camera and analyzed using an on-line controller (Photometrics). The size of the image corresponding to the contact area was obtained following the image from the center of the contact area to the edge and locating the first pixel at a distinguishably lower wavelength. Only spots which were circular (as judged by the appearance of Newton's rings) were analyzed for JKR purposes. The eccentricities were verified by measuring radii of curvature in orthogonal directions using a dovetail prism. All force data presented here have distance axes with "zero" corresponding to bare-mica/bare-mica contact, as measured during the initial thickness measurement. Other details of the SFA force and adhesion measurements are available.[23]

Results and Discussion

The adhesion properties of the DPPE-$(C_{16})_2$-Glu-C_2-Gly bilayers ("glycine bilayers") were measured in the SFA by first bringing the surfaces into light contact and then tracking the contact area as the surfaces were further loaded and eventually unloaded. Figure 4 shows contact radius (a) versus load (P) profiles for the initial contact of glycine bilayers in pure water (pH 5.6). Between each data point, the surfaces were loaded or unloaded at a constant rate of 0.02 dyn/s. A large hysteresis was observed between loading and unloading branches of the data, with a transition region of approximately constant a between the two branches (dotted circles). JKR fits (using eq 1) of the loading data have $W_l = 2.6$ mJ/m^2, on the order of values obtained from the JKR analysis of pull-off data in the SFA for uncharged phospholipid bilayers.[43] The glycine bilayers are less than 1% charged at pH 5.6 (based on fits to surface-force data, Figure 3), indicating that van der Waals forces are the dominant contributors to the weak adhesion on loading.

The constant-a region generally accompanies adhesion hysteresis, since additional tensile stress must be built up in the system to separate bonded surfaces on unloading.

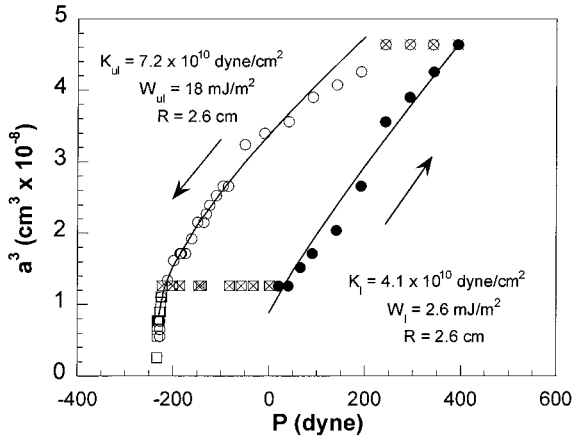

Figure 4. JKR load profiles for the initial contact of glycine bilayers in pure water (pH 5.6). Circles (high loading) and squares (low loading) are data taken at different spots with approximately the same R. Filled characters are loading data, unfilled are unloading data, and crosshatched characters are data in the transition region. Lines are least-squares fits to the JKR working equation for loading and unloading, with fit parameters listed in the insets. Transition data were not included in JKR fitting.

Once a critical tensile stress is achieved, the contact area begins to decrease, yielding a set of unloading data with a much higher adhesion ($W_{ul} = 18$ mJ/m^2 by eq 1) than the loading data. The fitted W_{ul} agrees very well with the value obtained from several independent pull-off measurements using eq 2 (18.7 mJ/m^2).[23] The difference in the fitted elastic constant for the unloading data (K_{ul}) versus the loading data (K_l) is noteworthy. As we explain below, we believe the difference is due to a spatially varying adhesion not accounted for in eq 1. To summarize, we ascribe the adhesion hysteresis to a series of molecular events: on loading, the surfaces are brought together by van der Waals forces; on unloading, the contact area remains constant until sufficient tensile stress is achieved to drive surface separation; and finally, the surfaces are damaged as the contact area decreases and eventually the surfaces jump apart. Upon varying the maximum load and the time held at the maximum load (from 1 to 60 min), we observed no changes in the pull-off force or the shape of the unloading curve.

As pH increased from 5.6 to 8.0 (in 1 mM KBr), the long-range repulsion between the glycine bilayers increases as the surfaces are charged (Figure 2). However, the attenuation in pull-off force (Figure 3) is not entirely due to the larger repulsive barrier provided by the electric double layer. The attractive part of the pull-off force ($F/R_{0,at}$), obtained by adding the electrostatic repulsion at contact to the measured pull-off force, also decreases with pH as interpenetration is encumbered.[23] The decrease in adhesion with pH is apparent in the JKR load profiles, accompanied by a diminished adhesion *hysteresis*. pH 6.8 profiles (Figure 5) are similar to those for the pH 5.6 case, with W_l being much lower than W_{ul} and K_{ul} about twice as large as K_l. However, the added electrostatic repulsion of these charged surfaces decreases the W_l from 2.6 mJ/m^2 at pH 5.6 to 0.14 mJ/m^2 for pH 6.8.

At pH 7.6 (Figure 6), the hysteresis is further diminished, with W_l remaining lower than W_{ul} and K_{ul} about twice as large as K_l. W_l is lowered further from the pH 6.8 case, in accord with the progressive charging of the bilayers. At pH 8.2 (Figure 7), the adhesion and adhesion hysteresis are completely removed and an identical, adhesion-free load profile is observed on loading and unloading. Here, the value for K is very close to values for

(42) Wood, J.; Sharma, R. *Langmuir* **1994**, *10*, 2307−2310.
(43) Marra, J.; Israelachvili, J. *Biochemistry* **1985**, *24*, 4608−4618.

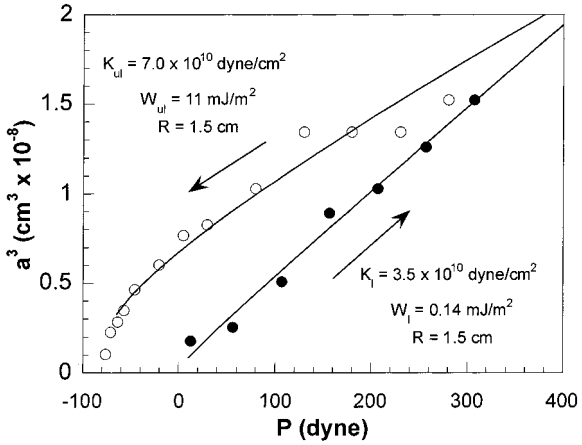

Figure 5. JKR load profiles for the initial contact of glycine bilayers in 1 mM KBr (pH 6.8). Filled circles are loading data, and unfilled circles are unloading data. Lines are least-squares fits to eq 1, with fit parameters listed in the insets.

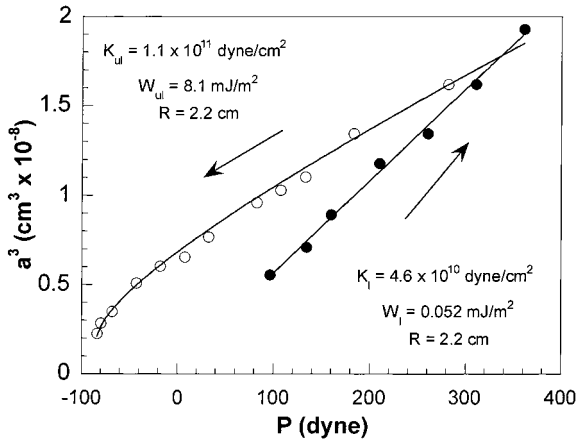

Figure 6. JKR load profiles for the initial contact of glycine bilayers in 1 mM KBr (pH 7.6). Filled circles are loading data, and unfilled circles are unloading data. Lines are least-squares fits to eq 1, with fit parameters listed in the insets.

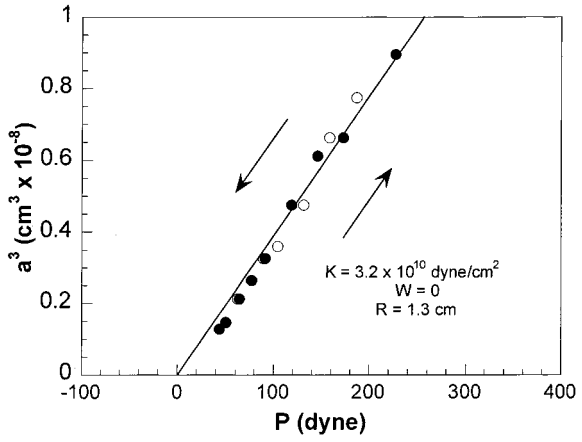

Figure 7. JKR load profiles for the initial contact of glycine bilayers in 1 mM KBr (pH 8.2). Filled circles are loading data, unfilled circles are unloading data. The line is a least-squares fit to eq 1, with fit parameters listed in the insets.

K_1 of the previous data, suggesting that K_1 represents the true elastic constant in all cases. These values also agree with those obtained in previous JKR experiments with the SFA.[34−36]

In an attempt to prevent the surface damage on unloading, we covalently bonded an OTE monolayer to the mica prior to the deposition of glycine amphiphiles using a plasma-modification method.[21,42] SFA force curves on the OTE/glycine bilayers show the same Derjaguin−Landau−Verwey−Overbeek (DLVO) behavior as the DPPE/glycine bilayers, but on separation the fracture plane is shifted from the bilayer/mica interface to the monolayer/monolayer interface, giving rise to a much larger adhesion on surface separation.[21] JKR load profiles for the OTE/$(C_{16})_2$-Glu-C_2-Gly bilayers (Figure 8) have a very large adhesion hysteresis, with $W_l = 0.11$ mJ/m^2 and $W_{ul} = 30$ mJ/m^2. These data allow us to study the effect of the greater energy dissipation during surface separation, while holding the surface chemistry constant.

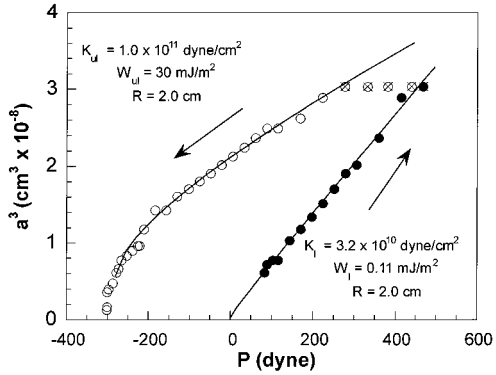

Figure 8. JKR load profiles for the initial contact of OTE/glycine bilayers in 1 mM KBr (pH 7.0). Filled circles are loading data, unfilled circles are unloading data. The line is a least-squares fit to eq 1, with fit parameters listed in the insets. Note the dramatically larger adhesion with the covalent OTE anchoring to mica.

Because the JKR theory disregards surface forces outside the contact area, it is only applicable in certain limits. Muller et al.[44] established a criterion for the applicability of JKR theory based on the parameter μ:

$$\mu = \frac{64}{3\pi}\left[\frac{W^2 R}{4\pi K^2 {D_0}^3}\right]^{1/3} \qquad (3)$$

where D_0 is the surface separation at contact (about 0.1 nm). JKR theory is valid for $\mu > 1$, and for our data, μ is in the range $11 < \mu < 245$.

Source of the Adhesion Hysteresis. In general, adhesion hysteresis can arise by several different mechanisms. One potential source is plastic deformation of the glue used to fix mica onto the silica lenses of the SFA; however, we failed to observe any hysteresis under nonadhesive conditions (pH = 8.2, Figure 7) in agreement with previous nonadhesive SFA−JKR measurements.[36] As further support, hysteresis absent at pH 8.4 emerged at the same spot after dropping the pH to 5.4 (separate experiment).

Attard and Parker[45,46] uncovered an ever-present source of adhesion hysteresis owing to elastic instabilities associated with rapidly varying but finite-ranged attractions between the surfaces. This effect is not accounted for in JKR theory, which assumes infinitely short-ranged contact forces. Self-consistent calculations based on a Lennard-Jones potential showed that this effect is significant for soft surfaces and/or strong adhesions and increases when the surfaces are subjected to greater maximum loads. In our system, measurements made with various maximum

(44) Muller, V. M.; Yushchenko, V. S.; Derjaguin, B. V. *J. Colloid Interface Sci.* **1980**, *77*, 91−101.
(45) Attard, P.; Parker, J. L. *Phys. Rev. A* **1992**, *46*, 7959−7971.
(46) Attard, P. *J. Phys. Chem. B* **2000**, 10635−10641.

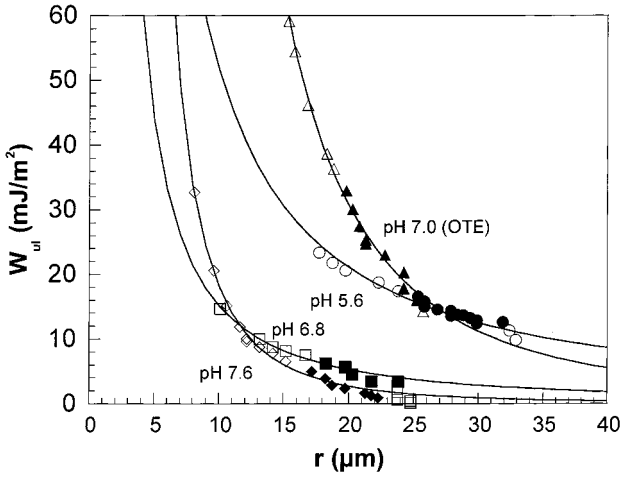

Figure 9. Apparent adhesion energy gradients for the unloading data presented using eq 3. Fits are made to the power-law expression $W = br^{-c}$ with fit parameters as follows: pH 5.6 (b = 1010, c = 1.29); pH 6.8 (b = 504, c = 1.52); pH 7.6 (b = 1930, c = 1.89); pH 7.0, OTE (b = 52 000, c = 2.48). Filled characters indicate regions of nearly constant crack velocity (v).

loads (pH 5.6) yielded equivalent unloading branches and pull-off forces; furthermore, the force profiles we measured have a long-range repulsion not present in the Lennard-Jones potential. For these reasons, we believe surface-jump instabilities are not the source of the large adhesion hysteresis we observe.

Ruling out these "mechanical hysteresis" mechanisms, we conclude that the hysteresis stems from some reorganization, bonding, or interpenetration of interfacial moieties after contact. The higher fitted elastic constant we observed for unloading data has been reported for JKR experiments on acid-treated PDMS lenses by Chaudhury and co-workers.[29,47] They ascribed the difference to a spatially variant adhesion on unloading, invalidating the constant W condition of eq 1. Here, we follow a similar analysis.

The adhesion energy at each data point on the unloading curve is obtained by inverting eq 1:

$$W(a) = \frac{1}{6\pi a^3 K_l}\left(\frac{a^3 K_l}{R} - P(a)\right)^2 \tag{4}$$

where K_l is the elastic constant from the loading branch. We emphasize that the pointwise use of the JKR expression is valid since we apply it each time at constant a, and therefore at constant W. The W versus a profile gives the radial (r) adhesion profile inside the original contact area, essentially by measuring W locally as the crack is driven inward from the edge of the original contact to the center. Figure 9 plots the apparent local adhesion with radius for the four systems presented earlier. Each demonstrates a sizable increase in W as the crack proceeds from edge to center during the unloading process. The apparent adhesion gradients are capably fit by a power-law expression.

For a spatially varying adhesion, the relationship between the pull-off force and G described by eq 2 is invalid. In this case, the stability criterion (establishing conditions for pull-off) is given by the following:[47]

$$\left(\frac{\partial(G - W)}{\partial a}\right)_P = 0 \tag{5}$$

where G is the elastic energy stored in the deformable substrates, and the subscript P indicates constant load. The spatial variation of elastic energy ($\partial G/\partial a$) can be obtained by differentiating the JKR working equation (eq 1) at constant load:

$$\left(\frac{\partial G}{\partial a}\right)_P = \frac{1}{2\pi}\left(\frac{a^2 K_l}{R^2} - \frac{P^2}{a^4 K_l}\right) \tag{6}$$

Here, we use the elastic constant obtained from the loading data, where $G = W$ and eq 1 is valid. Combining eq 5 with eq 6 (pull-off condition), we have

$$P_0 = -\left[\frac{a_0^6 K_l^2}{R^2} - 2\pi K_l a_0^4 \left(\frac{\partial W}{\partial a}\right)_0\right]^2 \tag{7}$$

which reduces to eq 2 in the absence of an adhesion gradient as expected. Equation 7 predicts that adhesion gradient effects augment the JKR result, giving larger pull-off forces than predicted by eq 1 for a given W.

The adhesion-gradient model is validated by comparing experimentally determined pull-off forces with those calculated by eq 7 (Table 1). Estimates of $\partial W/\partial a$ were made using the power-law expression fitted to the data of Figure 9. Calculations of the pull-off force from the adhesion energy gradient show a remarkable agreement with the calculated values, even with large variations in adhesion energy, curvature, and composition of the underlying LB matrix. The JKR prediction of the pull-off force from eq 2 underestimates the experimentally observed value by nearly an order of magnitude in some cases, since W is essentially averaged over the whole unloading curve. The numerical success of this model is strong evidence that adhesion gradient interpretation of the anomalous K values is correct and that the adhesion hysteresis stems from chemical reorganization or bonding after contact is made.

Source of the Adhesion Energy Gradient. Why does W increase on unloading? One possibility is that W increases with unloading rate as often observed in polymeric systems. While the unloading rate was constant in terms of force, the crack velocity (v) did increase substantially during unloading as the contact area shrunk. For the sphere-on-flat geometry of the SFA experiment, v is equal to the radial velocity of the contact perimeter, $-\mathrm{d}a/\mathrm{d}t$. This quantity can be calculated given the unloading rate ($-\mathrm{d}P/\mathrm{d}t$) and the experimentally obtained dependence of a on P:

$$v = -\frac{\mathrm{d}a}{\mathrm{d}t} = \left(\frac{\mathrm{d}a}{\mathrm{d}P}\right)\left(-\frac{\mathrm{d}P}{\mathrm{d}t}\right) \tag{8}$$

The Mark II SFA setup loads and unloads the surfaces at a constant rate $\mathrm{d}P/\mathrm{d}t$, so the slope of the a versus P plot is proportional to v. It is straightforward to locate regions on the a versus P plot that are highly linear and correspond to unloading measurements made at approximately constant v, typically on the order of $v = 0.5\ \mu$m/s. Despite the fact that the crack velocity is constant and fairly low here, W increases dramatically as shown by the filled characters in Figures 9 and 10. Therefore, it is unlikely that accelerations in unloading rate during the unloading process are responsible for the adhesion gradient. Experiments performed using faster unloading rates also did not produce significant changes in the measured adhesion or adhesion hysteresis.

(47) Silberzan, P.; Perutz, S.; Kramer, E. J.; Chaudhury, M. K. *Langmuir* **1994**, *10*, 2466−2470.

Table 1. Calculation of Pull-Off Force from Adhesion Gradient Data and Comparison to JKR Theory

	R (cm)	K_1 (dyn/cm^2 × 10^{10})	a_0 (μm)	$(\partial W/\partial a)_0$ (mJ/(m^2 μm))	$-P_0$ (eq 11) (dyn)	$-P_0$ JKR (dyn)	$-P_0$ expt (dyn)
pH 5.6	2.6	4.1	18	−1.8	239	87	228
pH 6.8	1.5	3.5	10	−2.3	75	23	77
pH 7.6	2.2	4.6	8.1	−11	117	11	111
pH 7.0 (OTE)	2.0	3.2	11	−32	308	21	301

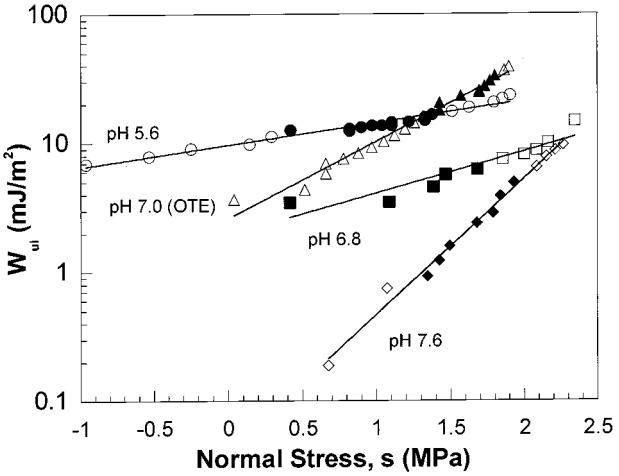

Figure 10. Local adhesion (W) versus normal stress (s) experienced at the point inside the original, fully loaded contact area equal to the contact radius at each point of the unloading curve. Fits are of the form $W = B\exp(-Cs)$ with the following fit parameters: pH 5.6 (B = 9.7 mJ/m^2, C = 0.39 MPa^{-1}); pH 6.8 (B = 2.0 mJ/m^2, C = 0.74 MPa^{-1}); pH 7.6 (B = 0.041 mJ/m^2, C = 2.4 MPa^{-1}); pH 7.0, OTE (B = 2.6 mJ/m^2, C = 1.4 MPa^{-1}). The filled characters represent portions of the data with an approximately constant crack velocity (v).

Stress-dependent surface rearrangements have also been cited as a source of adhesion hysteresis.[29,36,47] This could be particularly important here, since we may expect the interpenetration of glycine headgroups to be stress sensitive. JKR theory predicts a spatially varying normal stress profile, with maximum normal stress in the center of contact that decays gradually toward zero near the edge of the contact area. At this point, the normal stress becomes tensile, reflecting the additional contact area created by adhesive forces. The normal stress profile has the following functional form:[34]

$$s(r) = \frac{3Ka}{2\pi R}\left(1 - \frac{r^2}{a^2}\right)^{1/2} - \left(\frac{3WK}{2\pi a}\right)^{1/2}\left(1 - \frac{r^2}{a^2}\right)^{-1/2} \quad (9)$$

where s is the normal stress (positive in compression) and r is the radial position inside the circular contact area with radius a. For any stress-dependent, irreversible rearrangements that give rise to strong adhesion, the normal stress field of eq 9 will imprint an adhesion gradient at the point of highest loading. Then, on unloading, the crack will traverse through regions of increasingly adhesive material, from edge to center of the *original* contact area (of radius a). Assuming this mechanism, we can use eq 9 to calculate the maximum normal stress felt at each radius r within the original contact area and attempt to correlate it with the local adhesion calculated by eq 3 (Figure 10). G increases exponentially with normal stress in all cases, with the following functional form:

$$W = B\exp(-Cs) \quad (10)$$

where the prefactor B is related to the strength of adhesion and the decay constant C is a measure of the stress sensitivity. The values for B correlate well with the measured pull-off forces; they are much higher for the pH 5.6 and pH 7.0 (OTE) cases than for the pH 6.8 and pH 7.6 cases. Considering all unloading data, including the OTE-anchored case, C increases sharply through the titration of the carboxylic acids near pH 7.5, indicating that it has an electrostatic origin. Furthermore, the C for the OTE-anchored case (pH 7.0) does not depart from the trend for the DPPE-anchored layers, even though the OTE anchoring nearly doubles the adhesion. Changes in stress sensitivity must be brought about by changes in surface chemistry and not the integrity of the underlying bilayer or the overall adhesion.

While the stress-dependent model appears to be qualitatively correct, it fails to capture an important observation. It predicts a greater pull-off force with greater maximum load, since a greater extent of surface rearrangement will occur everywhere in the contact area at high loads. We have never observed any loading-history dependence on the pull-off force in this study; furthermore, the unloading branches of the a^3 versus P loading profiles coincide near the pull-off event. The thermodynamic analysis leading to eq 7 also would predict no change in pull-off force, since the adhesion gradient and the contact area at pull-off are both the same. This observation is in contrast to the work of Chen and co-workers,[36] who reported a strong increase in pull-off force with greater maximum load during SFA experiments on partially formed LB monolayers in air, which they ascribed to a stress-dependent interdigitation of alkane chains. In their case, the pull-off force was also a function of the unloading rate, another effect we did not observe. It is not surprising that our results differ in these ways, since we worked with LB bilayers deposited in the dense, liquid-condensed phase. Chen and co-workers observed no adhesion hysteresis for the contact of liquid-condensed monolayers, again supporting our contention that the adhesion hysteresis is due not to rearrangements of the supporting material but rather to interfacial bonding on contact.

We also must consider the possibility that some surface rearrangement may occur during the initial jump-to-contact. Impact forces felt during the jump-to-contact may give rise to more aggressive surface rearrangement than any extra loading would provide. In this case, there would be no dependence of loading history on the adhesion gradient or contact area at the pull-off condition, the key determinants of the measured pull-off force. We would expect some subtle changes in the overall shape of the a^3 versus P loading profiles far from the pull-off condition, but this was not rigorously tested. The pH dependence of the pull-off force (and adhesion gradient) can be explained by considering the softening of the jump-to-contact impact by repulsive electrostatic forces, leading to a lower extent of surface rearrangement at higher pH. In separate studies, Chaudhury and Owen[48] and Silberzan et al.[47] also observed load-independent pull-off forces for the contact of functionalized lenses of PDMS. While no definitive explanation was provided, both sources cited

(48) Chaudhury, M. K.; Owen, M. K. *J. Phys. Chem.* **1993**, *97*, 5722−5726.
(49) Chan, D. Y. C.; Pashley, R. M.; White, L. R. *J. Colloid Interface Sci.* **1980**, *77* (1), 283−285.

defects in the surface structure as possible sources of the adhesion hysteresis. AFM images of the bilayers do show some pinhole defects (about 100 nm in diameter), but defect-free regions the size of the SFA contact area (100−1000 μm^2) can be easily located.[23] Still, we cannot rule out contributions of subtle surface heterogeneities not detectable by AFM. A detailed analysis of impact forces on jump-to-contact in the SFA along with SFA measurements on other LB bilayers may shed some light on this issue.

Conclusions

Using the SFA, we have made detailed JKR-type measurements on LB bilayers in water. These LB bilayers were made of a synthetic glycine amphiphile that contains acid-dissociable and hydrogen-bonding groups, mimicking key aspects of the protein backbone. On contact at low pH, the surfaces have a pronounced, spatially varying adhesion hysteresis. While the source of the hysteresis is somewhat unclear, we postulate that the initial impact of the surfaces during jump-to-contact imprints a gradient of hydrogen bonds in the contact zone. The hysteresis is completely removed at high pH, ensuring that plastic deformation of the bilayer or supporting material does not contribute to the hysteresis. The most striking feature of these SFA-derived JKR data is the pH tunability of the adhesion. In addition to its significance from a physical chemistry standpoint, it allows surface forces to be directly manipulated during experiments and the impact on adhesion behavior to be assessed. These measurements set the stage for the use of the SFA in conjunction with LB-deposited peptide amphiphiles for quantitative, fundamental studies of bioadhesion in realistic environments.

Acknowledgment. The authors acknowledge Eastman Kodak Co., the Center for Interfacial Engineering, an NSF-sponsored Engineering Research Center at the University of Minnesota, and the National Science Foundation, Grant NSF-CTS-9616797.

LA011496G